Materials Today Nano 18 (2022) 100197

Contents lists available at ScienceDirect

Materials Today Nano

journal homepage: https://www.evise.com/profile/#/MTNANO/login

Photoinduced iodide repulsion and halides-demixing in layered perovskites☆

Y. Liu [a, b], M. Wang [b], A.V. Ievlev [a], A. Ahmadi [b], J.K. Keum [a, c], M. Ahmadi [b], B. Hu [b], O.S. Ovchinnikova [d, *]

[a] Center for Nanophase Materials Sciences, Oak Ridge National Laboratory, Oak Ridge, TN, 37830, United States
[b] Joint Institute for Advanced Materials, Department of Materials Science and Engineering, University of Tennessee, Knoxville, TN, 37996, United States
[c] Neutron Scattering Division, Oak Ridge National Laboratory, Oak Ridge, TN, 37830, United States
[d] Computational Science and Engineering Division, Oak Ridge National Laboratory, Oak Ridge, TN, 37830, United States

ARTICLE INFO

Article history:
Received 4 October 2021
Received in revised form
14 March 2022
Accepted 26 March 2022
Available online 5 April 2022

Keywords:
Metal halide perovskites
Phase segregation
Chemical distribution
Spacer cation effect

ABSTRACT

Mixing halides in metal halide perovskites (MHPs) is an effective approach for adjusting the MHPs bandgap for applications in tandem solar cells. However, mixed-halide (MH-) MHPs undergo light-induced phase segregation (LIPS) under continuous illumination. Therefore, understanding the mechanism of LIPS is necessary for developing stable MH-MHPs. In this work, we investigated LIPS in layered (L) MHPs and discovered a critical role of spacer cations in LIPS. Through probing chemical changes of LIPS, we unveil light-induced iodide repulsion and the formation of Br-rich-phase in illuminated regions during LIPS. This discovery also gives insight into the LIPS process in three-dimensional (3D) MHPs. By further investigating LIPS in 3D MHPs, we reveal that LIPS induces not only the formation of Br-rich and I-rich domains but also an overall change of halide distribution along the film thickness direction. Moreover, LIPS is more significant in bulk due to a larger population of photogenerated charge carriers. Overall, this study reveals the chemical mechanism of LIPS in MHPs and its potential effect on device performance, offering insight into understanding the LIPS mechanism and improving the stability of MHPs.

© 2022 Elsevier Ltd. All rights reserved.

The metal halide perovskites (MHPs) community has witnessed a rapid growth in the development of photovoltaics in the past decade, with a power conversion efficiency (PCE) increase from 3.8% to 25.7% in single-junction MHPs solar cells [1]. MHPs-based multijunction solar cells are now attracting enormous research interest to further boost the PCE of solar cells [2–5]. The possibility of tuning bandgap via adjusting and mixing halides [6] makes MHPs a promising candidate for applications in tandem solar cells with various structures, such as MHPs/MHPs [7], organic photovoltaics/MHPs [8], silicon/MHPs [2,4], and Copper Indium Gallium Selenide (CIGS)/MHPs multijunctions [9]. However, mixed-halide MHPs undergo phase segregation under photoillumination [10–12], which is detrimental to achieving stable photovoltaic devices. Therefore, understanding the process of light-induced phase separation (LIPS) will be a vital step for the application of mixed-halide MHPs in stable solar cells.

LIPS in MHPs were discovered by Hoke et al. [12], showing as a bandgap transition and photoluminescence (PL) redshift of mixed-halide MHPs under continuous illumination. Later, extensive research investigated how the LIPS affects optical properties of MHPs, such as emission, absorption, and so on [10,11,13–16]. LIPS originates from the formation of separated iodine (I^-) rich and bromine (Br^-) rich domains [10,11,13–17]. Therefore, LIPS is a chemical change due to halide migration driven by illumination. However, to date, direct observation of chemical changes due to LIPS in MHPs is missing. This is because LIPS is a reversible process [10,11,13–16], which recovers (remixing of separated I-domain and Br-domain) quickly in several minutes or hours when the samples

☆ Notice: This manuscript has been authored by UT-Battelle, LLC, under Contract No. DE-AC0500OR22725 with the U.S. Department of Energy. The publisher, by accepting the article for publication, acknowledges that the United States Government retains a non-exclusive, paid-up, irrevocable, worldwide license to publish or reproduce the published form of this manuscript, or allow others to do so, for the United States Government purposes. The Department of Energy will provide public access to these results of federally sponsored research in accordance with the DOE Public Access Plan (http://energy.gov/downloads/doe-public-access-plan).

* Corresponding author.
E-mail address: ovchinnikovo@ornl.gov (O.S. Ovchinnikova).

https://doi.org/10.1016/j.mtnano.2022.100197
2588-8420/© 2022 Elsevier Ltd. All rights reserved.

are stored in dark conditions, leading to challenges in probing the chemical changes directly. For this reason, irreversible LIPS processes will be good model systems to investigate chemical changes associated with LIPS, and hence, understand the underlying mechanism.

Currently, to improve the stability of MHPs, large spacer cations have been widely used, which lead to the formation of layered (L) MHPs structure and play roles in suppressing ion migration [18,19]. In addition to improving the stability of traditional 3D MHPs, L-MHPs have also established themselves as an excellent material for the application of the light-emitting field. In this regard, the emission color of L-MHP can also be controlled via mixing halides, resulting in mixed-halides L-MHP and consequently raising a question regarding the LIPS in mixed-halides L-MHP. However, to date, most research into LIPS mainly focused on 3D-MHPs [20–27], understanding of LIPS in layered MHPs is currently missing.

In this work, we investigated LIPS in layered MHPs (L-MHPs). We reveal that the spacer cation in L-MHPs plays a crucial role in LIPS, suggesting that adjusting cation is an effective approach for managing LIPS. In contrast to reversible LIPS in 3D-MHPs that recovers quickly under dark, LIPS in L-MHPs is irreversible and lasts for several days. This allows us to directly probe the chemical redistribution due to LIPS, which has not been thoroughly studied yet. Here, we use time-of-flight secondary ion mass spectrometry (ToF-SIMS) to probe the chemical distribution in MHPs. We find that illumination repels iodide ions and induces the formation of Br-rich in the illuminated region. Iodide repulsion is dependent on the light intensity, which results in a variation of halide distribution in both vertical and lateral directions of MHPs films. We further reveal that the chemical environment (e.g., oxygen penetration into MHPs) also affects LIPS. To comprehensively explore chemical changes due to LIPS in an operando condition, we illuminated a $MAPb(Br_{0.5}I_{0.5})_3$ (MA: methylammonium) film with a uniform white light LED and probed its chemical changes in both vertical and lateral directions. In addition to the formation of I-rich and Br-rich domains that have been discussed extensively, we also found a significant vertical halide redistribution due to LIPS, which can play critical roles in charge carrier transport, recombination, and extraction in these materials. Moreover, we discovered that LIPS occurs more significantly in the bulk of MHPs film than on the surface, which is probably due to a higher density of photogenerated charge carriers in bulk.

1. Results and discussions

We investigated LIPS in L-MHPs with different spacer cations, as shown in Fig. 1a–c. Although previous works investigated the effect of cations (e.g. MA, formamidinium (FA), cesium (Cs)) on LIPS, the choice of cation is very limited in 3D-MHPs, and these cations are still very similar in size and structure (e.g. MA *vs*. FA). In contrast, the choice of cation in L-MHPs is broader, offering a platform to better understand the role of cation in LIPS. We selected three spacer cations with different sizes and different functional groups (Fig. 1a–c), namely, ethylammonium (EA), n-butylammonium (BA), and phenethylammonium (PEA). Using these cations, we synthesized L-MHPs with an equal amount of bromide (Br) and iodide (I). The studied materials are $EA_2Pb(Br_{0.5}I_{0.5})_4$, $BA_2Pb(Br_{0.5}I_{0.5})_4$, and $PEA_2Pb(Br_{0.5}I_{0.5})_4$, abbreviated as EA-, BA-, and PEA-MHP, respectively. X-ray diffraction results of these three samples are shown in Fig. S1. Photoluminescence (PL) spectroscopy was first used to investigate LIPS in these L-MHPs. PL is a widely utilized spectroscopy to investigate LIPS phenomena in MHP [12,16]. LIPS shows as a continuous red-shift of PL peak due to the formation of separated Br-rich and I-rich phases; photogenerated carriers in the Br-rich phase transfer to the I-rich phase before recombining and emitting (as shown in Fig. S2). As a result, PL spectra predominantly (or only) show the emission peak of the I-rich phase (that is red-shifted compared to the original emission peak of the mixed Br–I phase), indicating chemical changes after LIPS.

In our PL measurement, we used a 375 nm laser with an intensity of 54.7 mW cm^{-2} to illuminate and excite the L-MHP samples. We observed a significant red-shift in the PL peak wavelength of EA-MHP under continuous illumination, as shown in Fig. 1d and e. This PL behavior of EA-MHP (Fig. 1d and e) is very similar to that of 3D-MHPs, confirming LIPS in this sample. The original PL intensity gradually decreases, and a newly emerged PL peak (in longer wavelength) corresponding to I-rich phases gradually increases. However, we only observed a small red-shift of ~1 nm in the PL peak position in the BA-MHP sample (Fig. 1f and g). In addition, we observed an emergence of a small peak at ~407 nm (insert of Fig. 1g) that corresponds to the PL emission of the pure-Br phase (i.e. BA_2PbBr_4) in BA-MHP. Accordingly, there is also LIPS in the BA-MHP sample, which is evidenced by the formation pure-Br phase (insert of Fig. 1g). However, the LIPS in BA-MHP is very weak as the overall changes in the PL spectrum of BA-MHP are very small. In drastic contrast to EA-MHP and BA-MHP, we did not observe any obvious PL change in PEA-MHP (Fig. 1h and i), suggesting the PEA-MHP is stable to illumination and does not show any signs of LIPS in our measurement condition.

We further explored the effect of illumination intensity on the LIPS in these three L-MHPs. The PL spectra of three L-MHPs with different excitation intensities are shown in Figs. S3–S5. We used a lower intensity (12.5 mW cm^{-2}) and a higher intensity (155 mW cm^{-2}) 375 nm laser to illuminate L-MHP samples and studied their PL behavior as a function of time. All observed phenomena in the three L-MHPs samples are similar to those we observed in Fig. 1: (1) EA-MHP shows a red-shift of PL peak, (2) BA-MHP shows a rise of new PL peak around 407 nm, corresponding to pure-Br-phase BA-MHP (a reference PL result of pure-Br-BA-MHP, BA_2PbBr_4 sample, is shown in Fig. S6), and (3) PEA-MHP shows no obvious change in the PL spectrum after 30 min continuous illumination. In the EA-MHP sample, the red-shift in PL is weaker under lower illumination intensity (Figs. S3a–b) and stronger under higher illumination intensity (Figs. S3c–d). This suggests that LIPS in EA-MHP is illumination-intensity-dependent. In the BA-MHP sample, the emergence of a PL peak around 407 nm indicating a Br-rich-phase [28] is also illumination-intensity-dependent (shown in the inserts of Figs. S4b and S4d), suggesting the LIPS in BA-MHP is also illumination-intensity-dependent. The illumination-intensity-dependency of LIPS in EA-MHP and BA-MHP samples is consistent with previous observations in 3D-MHPs [27], indicating the similarity of LIPS between L-MHPs and 3D-MHPs. Therefore, the underlying mechanism of LIPS in 3D-MHPs and L-MHPs can be similar, suggesting that understanding LIPS in L-MHPs will also offer useful knowledge for LIPS in 3D-MHPs.

Noteworthily, no obvious change in the PEA-MHP sample is observed even with the highest illumination intensity here (Figs. S5c–d), suggesting PEA-MHP shows higher resistance to LIPS than both EA-MHP and BA-MHP, indicating the role of spacer cation in the stability of L-MHP.

Interestingly, under higher illumination intensity (155 mW cm^{-2}), a peak around 450 nm rises in the EA-MHP PL spectrum (Fig. S3d), which is associated with the pure-Br EA-MHP (i.e. EA_2PbBr_4, a reference PL result of EA_2PbBr_4 is shown in Fig. S6) and is consistent with the behavior of BA-MHP. To confirm the formation of pure-Br EA-MHP, we further increased the illumination intensity to 570 mW cm^{-2} (375 nm laser) to study the evolution of the EA-MHP PL spectrum. As shown in Fig. S7, we observed an obvious PL peak around 450 nm after 30 min illumination, verifying the formation of pure-Br-phase during LIPS in EA-MHP. In

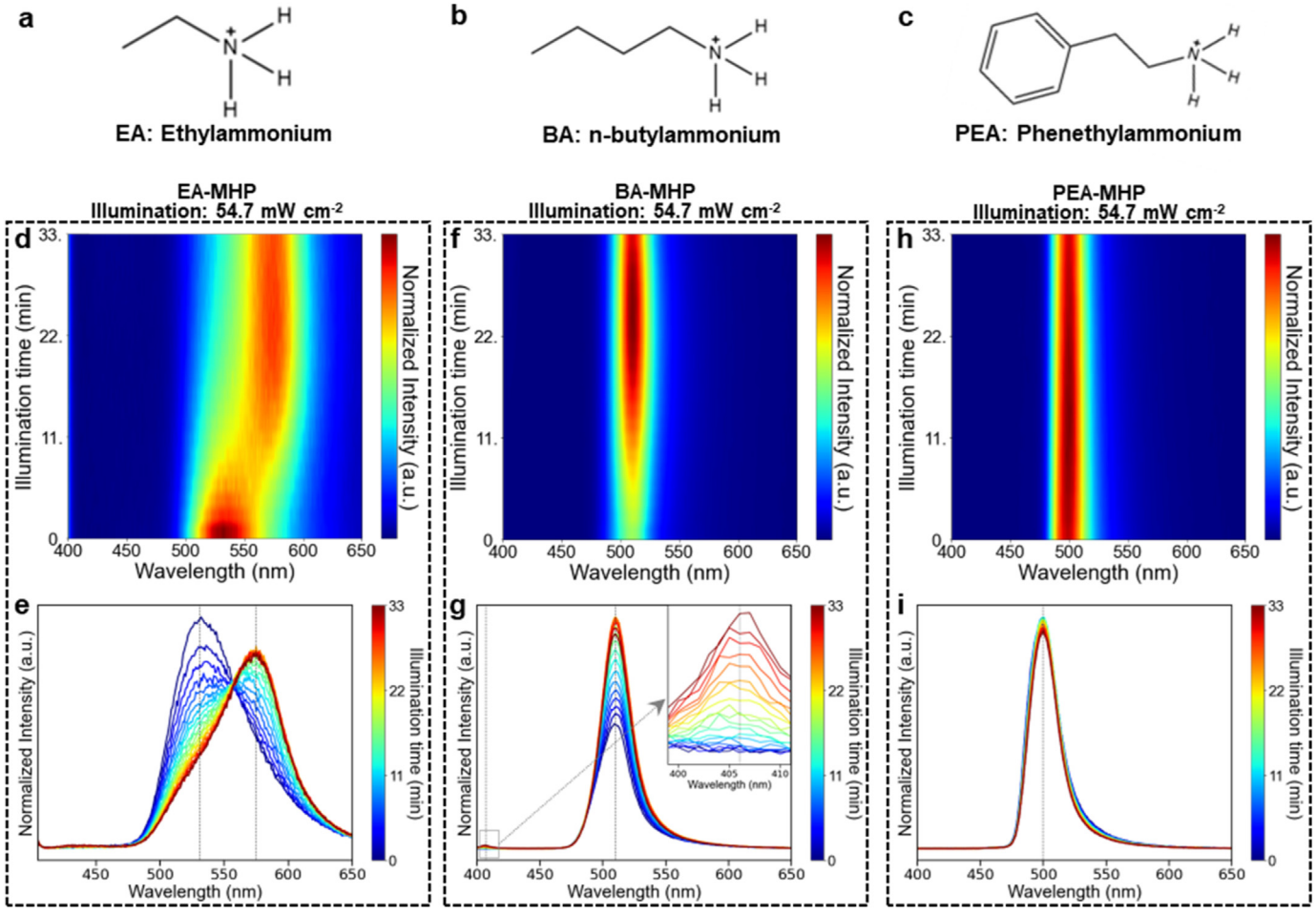

Fig. 1. **a-c,** molecular structures of three spacer cations, **a,** EA; **b,** BA; **c,** PEA. **d, f, h,** contour images of PL evolution under continuous illumination of three L-MHP; **d,** EA-MHP; **f,** BA-MHP; **h,** PEA-MHP. **e, g, i,** PL spectra corresponding to contour images in **d, f, h,** respectively.

addition, the 1-h evolution of EA_2PbBr_4 and BA_2PbBr_4 in Fig. S6 suggests no or negligible degradation of these two samples during PL measurements, which also implicates that the degradation effect on the LIPS observed in the mixed halides L-MHPs is negligible.

A distinct difference between LIPS in L-MHPs (EA- and BA-MHPs) and 3D-MHPs is its reversibility: LIPS in 3D-MHPs is reversible while LIPS in L-MHPs is irreversible. As shown in Fig. S9, LIPS-induced PL changes are still very stable after keeping the L-MHPs samples under dark conditions for 1 h. Note that the effect of spacer cation on LIPS in L-MHPs was also revealed in a recent study [29], where the authors also observed irreversible LIPS when the BA-MHP is exposed to air. However, the LIPS is reversible when the BA-MHP film is protected by a poly(methyl methacrylate) (PMMA) layer [29]. This suggests that the environment affects the LIPS process, either because (1) exposure to air induces BA-MHP degradation leading to irreversible LIPS [29] or (2) humidity and/or oxygen (etc.) affect the reversibility of LIPS as revealed by several previous studies [14,30,31]. It is well known that LIPS is a chemical phenomenon that is associated with photoinduced ion redistribution. However, owing to the reversibility of LIPS in 3D-MHPs, it is challenging to directly detect the chemical changes due to LIPS. Thus, most previous studies only focused on investigating the changes in optical properties due to LIPS. In contrast, irreversible LIPS in L-MHPs offers us an opportunity to directly detect chemical changes, allowing us to understand the exact chemical changes and the detailed mechanism of LIPS. Irreversible LIPS in L-MHPs is likely due to the higher activation energy for ion migration in L-MHPs; therefore, automatic ion redistribution under dark conditions is inhabited in L-MHPs.

Next, we study the nature of chemical changes in L-MHPs due to LIPS using ToF-SIMS. We used a rectangular-shape laser spot (375 nm) to illuminate the L-MHPs samples, where the rectangular width is less than the maximum field of view of ToF-SIMS (500 × 500 μm). Therefore, we can cover both the illuminated and non-illuminated regions in a ToF-SIMS dataset, and this allowed us to directly compare the chemical changes associated with illumination. The rectangular-shape illumination is shown in Fig. 2a, where the blue stripe represents the illuminated region. Since we only observed LIPS in EA-MHP and BA-MHP, we only discuss chemical changes in EA-MHP and BA-MHP here. After laser illumination (30 min), we transferred the samples to ToF-SIMS for chemical characterization.

To explore the effect of illumination intensity on chemical changes, we varied the laser intensity and performed chemical characterization after various intensity illumination. According to the Beer-Lambert law, we expect the chemical change in the vertical direction to be depth-dependent due to the decay of laser intensity inside the materials. Note that the laser used here is not perfectly uniform, and the intensity of this laser decays from the middle to the edge of the rectangular due to the Gaussian profile of the laser intensity within the laser spot. Therefore, depending on

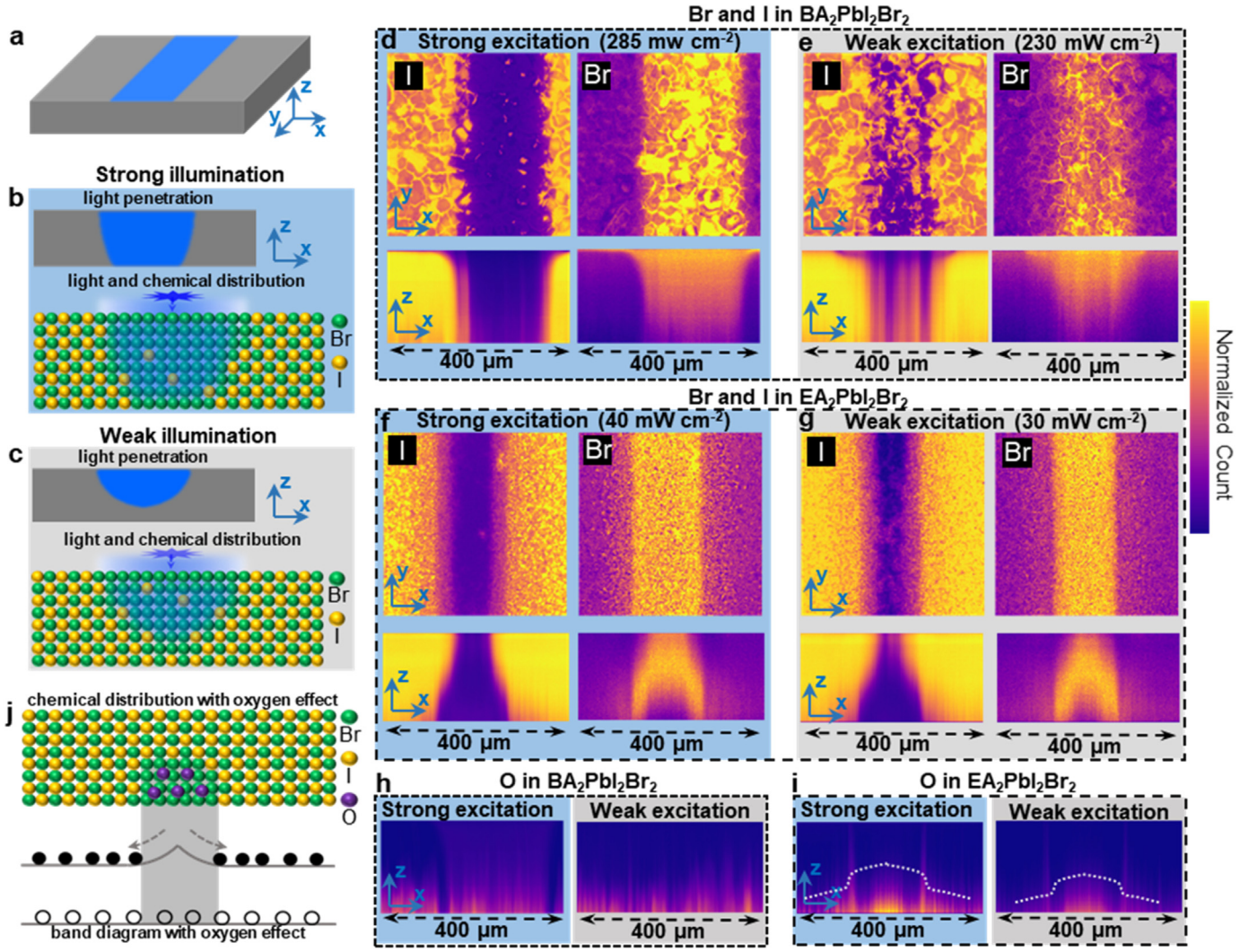

Fig. 2. **a,** schematic diagram of stripe-shape illumination, the blue stripe represents illuminated region. **b,** cross-section view of expected illumination condition under a strong illumination (top) and corresponding halide distribution. **c,** cross-section view of expected illumination condition under a weak illumination (top) and corresponding halide distribution. **d,** I and Br distributions in BA-MHP under strong illumination. **e,** I and Br distributions in BA-MHP under weak illumination. **f,** I and Br distributions in EA-MHP under strong illumination. **g,** I and Br distributions in EA-MHP under weak illumination. In **d-g**, the top row is integrated top view, and the bottom row is integrated cross-section-view. **h,** oxygen distribution in BA-MHP after strong and weak illumination. **i,** oxygen distribution in EA-MHP after strong and weak illumination.

whether or not the laser can penetrate the MHP films, the expected illumination conditions and corresponding resultant chemical distributions under strong illumination (can penetrate) and weak illumination (cannot penetrate) are schematically shown in Fig. 2b and c, respectively. Previous works revealed that laser illumination could expel iodide in MHPs into solvent when the MHP sample was in contact with a solvent [32]. Our PL results show that strong laser illumination can lead to the formation of pure Br-phase (the appearance of PL from pure Br-phase, Fig. 1 and Fig. S7), also implies an iodide-repulsion effect. Therefore, we speculate that the laser treatment results in an I-deficient region in the illumination region. Based on this analysis, the expected chemical distributions after strong and weak illuminations are also schematically shown in Fig. 2b and c.

ToF-SIMS results of Br and I distributions in BA-MHP and EA-MHP samples are shown in Fig. 2d–g. The top row of each panel shows the integrated top view (x-y) chemical distribution maps, and the bottom row of each panel shows the integrated cross-section view (x-z) chemical distribution maps; the coordinate (x-y or x-z) is labeled at the bottom right of each row. In Fig. 2d, we observed an I-deficient (top right of Fig. 2d) and Br-rich (top left of Fig. 2d) stripe in the illuminated regions, suggesting that illumination expels iodide and results in I-deficient and Br-rich (IDBR) regions. In the cross-section view (bottom row of Fig. 2d), we find that I-deficient and Br-rich region is slightly broader at the top (near the surface), which is consistent with our expectation in Fig. 2b, suggesting laser penetration indeed plays a role in LIPS chemical changes. The laser of the stripe edge is too weak to penetrate the film, and hence, only affects chemical changes near the film surface. When we reduce the laser intensity, the laser of the stripe middle is not able to penetrate the film and only affects the chemical changes near the surface. This case is shown in Fig. 2e; from the cross-section view of Br and I distribution (bottom row of Fig. 2e), we can see that the IDBR effect near the bottom middle is very weak. In addition, the overall chemical distribution in this case (bottom row of Fig. 2e) is perfectly consistent with our schematic analysis in Fig. 2c. Also, the IDBR effect is apparently weaker under the weaker illumination (Fig. 2e) than that under stronger illumination (Fig. 2d), suggesting that the iodide-repulsion effect is light-intensity-dependent.

The EA- and BA- MHPs were also checked by scanning electron microscopy after stripe illumination, which shows a sharper contrast between illuminated and nonilluminated regions in EA-MHP, as shown in Fig. S8. This is because more significant LIPS leads to a large composition variation between illuminated and nonilluminated regions in EA-MHP.

The IDBR stripe in the illuminated region is also observed in EA-MHP, indicating that illumination similarly repels iodide in the EA-MHP sample. However, the cross-section view (bottom row of Fig. 2f and g) reveals significantly different distributions of the chemicals. One can see the broadening of the IDBR region close to the bottom interface with the substrate. This IDBR distribution is inconsistent with predicted ion distribution (Fig. 2b and c), which implicates unconsidered factors affecting the iodide repulsion during illumination.

Interestingly, in the cross-section view oxygen distribution maps in Fig. 2h and i (oxide ion from glass substrate can penetrate to the thin MHPs), we observed a relatively uniform oxygen distribution in BA-MHP (Fig. 2h) without any correlation with the IDBR region. In contrast, the oxygen distribution in EA-MHP (Fig. 2e) shows correspondence to the IDBR region and is dependent on light intensity. This correlation between oxygen distribution and the IDBR region (as marked in Fig. 2e) indicates that oxide ion in MHP also affects iodide repulsion. It has been previously revealed that oxygen in MHPs can lead to an up-shift of the conduction band but has a negligible effect on the valence band [33]. Accordingly, an oxygen-rich condition (which is near the substrate and in the illuminated region, as shown in Fig. 2i) in EA-MHP will lead to an electronic band bending and results in a hole-rich area in the corresponding region, as schematically shown in Fig. 2j. It is revealed that the hole carriers have a role in repulsion iodides in MHPs [32,34]. Therefore, we propose that the correlation between oxygen distribution and the IDBR region is due to oxygen-induced hole accumulation, which repels iodide. In summary, under illumination, oxygen from the substrate penetrates the EA-MHP and leads to a local hole-rich environment, which results in iodide repulsion (we refer to this phenomenon as oxygen-induced iodide repulsion). This oxygen-induced iodide repulsion, together with light-induced iodide repulsion, results in the abnormal IDBR regions in EA-MHP (Fig. 2f and g).

The difference in oxygen distribution in BA-MHP (Fig. 2h) and EA-MHP (Fig. 2i) also indicates that spacer cations (e.g. BA vs. EA) affect on oxygen penetration in MHPs, which is important to MHP performance and stability. Therefore, the role of spacer cation in ion

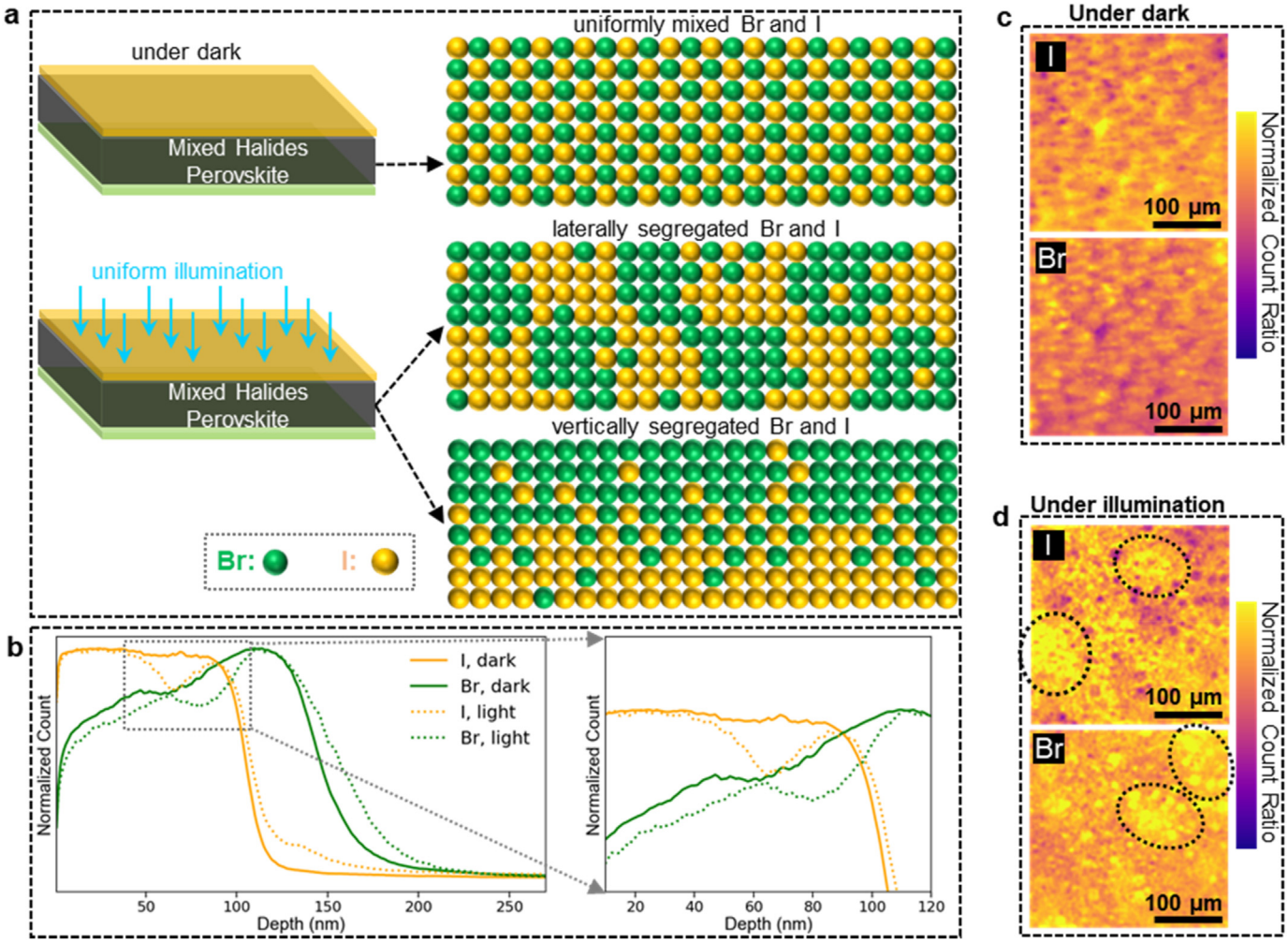

Fig. 3. a, schematic diagram of expected illumination condition and halide distribution under dark and operando condition. **b,** the depth profile of iodide, bromide, and oxygen distribution in $MAPb(Br_{0.5}I_{0.5})_3$ under dark (solid lines) and illumination (dashed lines), a significant change in Br and I distribution due to illumination is observed. **c,** lateral distribution of I and Br under dark was shown as the ratio; the ratio was calculated as: e.g. iodide ratio, R_I = (I count)/(I count + Br count). **d,** lateral distribution of I and Br under illumination. Microscale I and Br segregation is observed under illumination (**d**) compared to those under dark (**c**), the I-rich and Br-rich regions are marked by circles in the I ratio map and Br ratio map in (**d**), respectively.

migration and stability of MHPs is worth further exploring in the future. Note that a recent study has explored the effect of spacer cation on ion migration, revealing that the suppression of phase segregation can be rationalized by increased activation energy for halide migration in low dimensional mixed halide perovskite films [35]. Therefore, the effect of spacer cation on the activation energy of ion migration is a possible reason for the difference in LIPS in these L-MHPs films. Regarding the effect of oxygen on LIPS, several groups also performed insightful investigations before. Fan et al. revealed that oxygen passivation could suppress LIPS, and an oxygen environment can lead to the recovery of phase-separated MHPs to the uniform state [30]. Ruf et al. found that the LIPS is enhanced when the perovskite films are exposed to an oxygen environment [31]. Tang et al. observed negligible difference in LIPS when the perovskite films were exposed to air and vacuum [14]. Moreover, for oxygen from the substrate, we proposed an indirect mechanism of how it affects the LIPS, as discussed above. Similarly, Kamat et al. investigated the impact of TiO_2 and ZrO_2 on the phase segregation in MHPs [36]; the authors observed LIPS in MHPs deposited on TiO_2 but not on the ZrO_2 substrate and suggested that the reason for LIPS is the hole accumulation in MHPs film, which is consistent with our proposed mechanism. Accordingly, further efforts are also necessitated to clarify the effect of the environment (e.g. oxygen) and substrates on the LIPS in MHPs.

It has been suggested that the formation of Br-rich and I-rich domains (as schematically shown in Fig. 3a) due to LIPS detrimentally affects the photovoltaic performance of MHPs by trapping charge carriers in I-domains [37]. Our chemical investigations show that LIPS can also induce a chemical change along the vertical direction of MHP films (as schematically shown in Fig. 3a), which will significantly affect charge carrier transport and extraction. In the LIPS studies above (Figs. 1–2), we illuminated MHP samples with a laser, which is not a uniform illumination. Thus, an IDBR region corresponding to the illuminated region formed due to light-induced iodide repulsion. However, in an operando condition, MHP films should be under a uniform illumination (that is, the whole MHP film is under illumination). Therefore, we next systematically investigate light-induced chemical distribution change in MHP under a uniform illumination in order to understand light-induced chemical changes in operando devices. We utilized a built-in white LED light panel in the ToF-SIMS chamber to illuminate the MHP samples; as the LED illumination area is much larger than the MHP sample size, this illumination can be treated as a uniform illumination.

We performed ToF-SIMS measurements on a $MAPb(Br_{0.5}I_{0.5})_3$ sample under both dark and LED illumination to understand light-induced chemical changes. ToF-SIMS results are shown in Fig. 3b–d. In the ToF-SIMS depth profiles (Fig. 3b), we clearly observed a difference in Br and I distribution between dark (solid curves) and illumination conditions (dashed curves), indicating light-induced halide redistribution along the vertical direction. We also simultaneously investigated halide distribution in the lateral direction, shown as chemical maps in Fig. 3c and d. Under illumination, we clearly observed microscale Br-rich and I-rich domains (Fig. 3d) in comparison with dark conditions (Fig. 3c), suggesting the light-induced formation of Br-rich and I-rich phases. Therefore, LIPS results in not only the formation of Br-rich and I-rich domains but also overall changes in halide distribution along the vertical direction. Noteworthily, effective charge carrier transport in an MHP device is along the vertical direction, and therefore, LIPS-induced vertical halide redistribution will affect charge carrier transport and MHP devices' performance. This is consistent with recent literature [38], which revealed that an improper energy alignment due to LIPS is responsible for the photovoltaic performance loss [38]. Here, our results on vertical redistribution of halides elucidate the chemical origin of this improper energy alignment. The energy alignment related to halide redistribution will affect charge carrier transport, and consequently, photovoltaic performance of MHPs [38].

In the depth profiles in Fig. 3b, we explicitly see that light-induced changes in halide distribution are mainly located at the bulk of MHP film, suggesting that MHP's bulk undergoes the most significant LIPS. Therefore, we further analyzed the lateral halide segregation in the bulk and surface of MHP separately. As shown in Fig. S10a, we show the lateral distribution of Br and I near the surface and bulk of the MHP film. Consistent with our speculation, a more significant light-induced halide segregation (exhibits as the formation of Br-rich and I-rich domains) is seen in bulk (Fig. S10c) than near the surface (Fig. S10b). Since it has been revealed that halide migration and segregation are associated with charge carriers [32,34], the more significant LIPS in bulk is probably because of a larger population of photogenerated charge carriers in bulk than on the surface.

2. Conclusions

In conclusion, we investigated LIPS in L-MHPs, unveiling that spacer cation plays a crucial effect in LIPS. We observed irreversible LIPS in L-MHPs; this irreversible LIPS offers an opportunity to directly investigate chemical redistribution due to LIPS, which is challenging in 3D MHPs that show quickly reversible LIPS behavior. Our chemical characterization of LIPS in L-MHPs revealed an iodide-repulsion effect and consequently the formation of pure-Br-phase or extremely Br-rich phase in the illuminated region, where iodide repulsion is dependent on light intensity and chemical environment (e.g. oxygen penetration into MHPs affect iodide repulsion process). In order to understand chemical redistribution due to LIPS in an operando condition, we illuminated a $MAPb(Br_{0.5}I_{0.5})_3$ film using a uniform white LED light. In addition to the formation of I-rich and Br-rich domains (that is a generally believed mechanism of LIPS), we discovered that LIPS also leads to a significant vertical chemical redistribution, which is critical to charge carrier transport and extraction in MHPs devices. Moreover, we discovered that LIPS is more significant in the bulk of the MHP film, which is probably due to a large population of photogenerated charge carriers in bulk. Overall, by directly characterizing chemical changes due to LIPS, we, for the first time, revealed the chemical changes associated with LIPS in MHPs, which is the key to understanding LIPS mechanism and developing stable mixed-halides MHPs. Our studies about the role of spacer cation in LIPS and extrinsic ion penetration also offer insight into improving the stability of MHPs.

3. Methods

3.1. Materials preparation

The metal halide perovskites samples were synthesized on Swiss glass slides. The glass slides were precleaned using deionized water, acetone, and isopropanol. $EA_2Pb(Br_{0.5}I_{0.5})_4$ were synthesized by spin-casting a precursor (1 M PbI_2 and 2 M EABr in d dimethyl sulfoxide) at 3000 rpm; then, the spin-casted film was annealed at 100 °C for 10 min $BA_2Pb(Br_{0.5}I_{0.5})_4$ were synthesize by spin-casting a precursor (1 M PbI_2 and 2 M BABr in d dimethyl sulfoxide) at 3000 rpm, then, the spin-casted film was annealed at 100 °C for 10 min $PEA_2Pb(Br_{0.5}I_{0.5})_4$ were synthesize by spin-casting a precursor (1 M $PbBr_2$ and 2 M PEAI in d dimethyl sulfoxide) at 3000 rpm, then, the spin-casted film was annealed at 100 °C for 10 min. $MAPb(Br_{1.5}I_{1.5})$ was synthesized by spin-casting a precursor (0.8 M lead (II) acetate trihydrate, 1.2 M MAI, and 1.2 M MABr in

dimethylformamide) at 3000 rpm; then, the spin-casted film was annealed at 100 °C for 30 min. Precursor preparation, film spin-casting, and annealing were performed in an N_2-filled glove box.

3.2. Photoluminescence (PL) measurement

PL measurements were performed by using Horiba Fluorolog-3 spectrometer. The excitation source is from a 375 nm continuous-wave laser combined with the focus lens. Filters were used to adjust laser intensity and laser shape.

3.3. Time-of-flight secondary ion mass spectrometry (ToF-SIMS)

ToF-SIMS measurements were performed using ToF-SIMS.5.NSC instrument (ION.TOF GmbH. Germany). Experiments were carried out in negative ion detection mode using Bi_3^+ primary and Cs^+ sputter ion sources. Bi_3^+ primary ions source with the energy of 30 keV, current of 0.5 nA, and spot size of ~120 nm was used to generate secondary ions of the studied sample. A sputter source with the energy of 500 eV, current of 70 nA, and spot size ~20 μm was used for depth profiling and removing of the significant amount of material for chemical studies in bulk. Measurements were carried out in non-interlaced mode, where each chemical scan (500 × 500 μm, 256 × 256 px, ~20 s duration) with the primary source was followed by sputtering (750 × 750 μm, 4 s duration). Time-of-flight mass analyzer was used to analyze negative secondary ions with mass resolution $m/\Delta m = 100-500$.

Author contributions

Y.L. conceived the project and O.S.O directed the experiments. Y.L. prepared the samples. Y.L. performed PL measurements with help from M.W.. A.A. performed the partial synthesis and PL experiment with help from M.A. and Y.L.. A.V.I. performed ToF-SIMS measurement. J.K.K. performed X-ray diffraction measurement. All authors contributed to discussions of the results and manuscript.

Declaration of competing interest

The authors declare that they have no known competing financial interests or personal relationships that could have appeared to influence the work reported in this paper.

Acknowledgments

The work (materials synthesis and ToF-SIMS characterization) was supported by the Oak Ridge National Laboratory's Center for Nanophase Materials Sciences, a U.S. Department of Energy, Office of Science User Facility and through the DOE Office of Science Research Program for Microelectronics Codesign (sponsored by ASCR, BES, HEP, NP, and FES) through the Abisko Project, PM Robinson Pino (ASCR). This work uses instrumentation within ORNL's Materials Characterization Core provided by UT-Battelle, LLC under Contract No. DE-AC05-00OR22725 with the U.S. Department of Energy. M.A. acknowledges support from National Science Foundation (NSF), Award Number # 2043205.

Appendix A. Supplementary data

Supplementary data to this article can be found online at https://doi.org/10.1016/j.mtnano.2022.100197.

References

[1] NREL: Best Research-Cell Efficiencies, Available at: https://www.nrel.gov/pv/assets/pdfs/best-research-cell-efficiencies.20200925.pdf, 2020. (Accessed April 2022).
[2] B. Chen, J.Y. Zhengshan, S. Manzoor, S. Wang, W. Weigand, Z. Yu, G. Yang, Z. Ni, X. Dai, Z.C. Holman, Blade-coated perovskites on textured silicon for 26%-efficient monolithic perovskite/silicon tandem solar cells, Joule 4 (4) (2020) 850–864.
[3] E. Lamanna, F. Matteocci, E. Calabrò, L. Serenelli, E. Salza, L. Martini, F. Menchini, M. Izzi, A. Agresti, S. Pescetelli, Mechanically stacked, two-terminal graphene-based perovskite/silicon tandem solar cell with efficiency over 26%, Joule 4 (4) (2020) 865–881.
[4] Y. Hou, E. Aydin, M. De Bastiani, C. Xiao, F.H. Isikgor, D.-J. Xue, B. Chen, H. Chen, B. Bahrami, A.H. Chowdhury, Efficient tandem solar cells with solution-processed perovskite on textured crystalline silicon, Science 367 (6482) (2020) 1135–1140.
[5] J. Xu, C.C. Boyd, J.Y. Zhengshan, A.F. Palmstrom, D.J. Witter, B.W. Larson, R.M. France, J. Werner, S.P. Harvey, E.J. Wolf, Triple-halide wide–band gap perovskites with suppressed phase segregation for efficient tandems, Science 367 (6482) (2020) 1097–1104.
[6] A. Sadhanala, S. Ahmad, B. Zhao, N. Giesbrecht, P.M. Pearce, F. Deschler, R.L.Z. Hoye, K.C. Gödel, T. Bein, P. Docampo, S.E. Dutton, M.F.L. De Volder, R.H. Friend, Blue-green color tunable solution processable organolead chloride–bromide mixed halide perovskites for optoelectronic applications, Nano Lett. 15 (9) (2015) 6095–6101.
[7] G.E. Eperon, T. Leijtens, K.A. Bush, R. Prasanna, T. Green, J.T.-W. Wang, D.P. McMeekin, G. Volonakis, R.L. Milot, R. May, Perovskite-perovskite tandem photovoltaics with optimized band gaps, Science 354 (6314) (2016) 861–865.
[8] Y. Liu, Y. Chen, Integrated perovskite/bulk-heterojunction organic solar cells, Adv. Mater. 32 (3) (2020) 1805843.
[9] H. Shen, J. Peng, D. Jacobs, N. Wu, J. Gong, Y. Wu, S.K. Karuturi, X. Fu, K. Weber, X. Xiao, Mechanically-stacked perovskite/CIGS tandem solar cells with efficiency of 23.9% and reduced oxygen sensitivity, Energy Environ. Sci. 11 (2) (2018) 394–406.
[10] M.C. Brennan, S. Draguta, P.V. Kamat, M. Kuno, Light-induced anion phase segregation in mixed halide perovskites, ACS Energy Lett. 3 (1) (2017) 204–213.
[11] D.J. Slotcavage, H.I. Karunadasa, M.D. McGehee, Light-induced phase segregation in halide-perovskite absorbers, ACS Energy Lett. 1 (6) (2016) 1199–1205.
[12] E.T. Hoke, D.J. Slotcavage, E.R. Dohner, A.R. Bowring, H.I. Karunadasa, M.D. McGehee, Reversible photo-induced trap formation in mixed-halide hybrid perovskites for photovoltaics, Chem. Sci. 6 (1) (2015) 613–617.
[13] O. Hentz, Z. Zhao, S. Gradecak, Impacts of ion segregation on local optical properties in mixed halide perovskite films, Nano Lett. 16 (2) (2016) 1485–1490.
[14] X. Tang, M. van den Berg, E. Gu, A. Horneber, G.J. Matt, A. Osvet, A.J. Meixner, D. Zhang, C.J. Brabec, Local observation of phase segregation in mixed-halide perovskite, Nano Lett. 18 (3) (2018) 2172–2178.
[15] Y. Zhao, P. Miao, J. Elia, H. Hu, X. Wang, T. Heumueller, Y. Hou, G.J. Matt, A. Osvet, Y.-T. Chen, Strain-activated light-induced halide segregation in mixed-halide perovskite solids, Nat. Commun. 11 (1) (2020) 1–9.
[16] W. Mao, C.R. Hall, S. Bernardi, Y.-B. Cheng, A. Widmer-Cooper, T.A. Smith, U. Bach, Light-induced reversal of ion segregation in mixed-halide perovskites, Nat. Mater. (2020) 1–7.
[17] J. Cho, P.V. Kamat, Photoinduced phase segregation in mixed halide perovskites: thermodynamic and kinetic aspects of Cl–Br segregation, Adv. Opt. Mater. (2020) 2001440.
[18] Y. Lin, Y. Bai, Y. Fang, Q. Wang, Y. Deng, J. Huang, Suppressed ion migration in low-dimensional perovskites, ACS Energy Lett. 2 (7) (2017) 1571–1572.
[19] X. Xiao, J. Dai, Y. Fang, J. Zhao, X. Zheng, S. Tang, P.N. Rudd, X.C. Zeng, J. Huang, Suppressed ion migration along the in-plane direction in layered perovskites, ACS Energy Lett. 3 (3) (2018) 684–688.
[20] P. Nandi, C. Giri, D. Swain, U. Manju, S.D. Mahanti, D. Topwal, Temperature dependent photoinduced reversible phase separation in mixed-halide perovskite, ACS Appl. Energy Mater. 1 (8) (2018) 3807–3814.
[21] S.J. Yoon, M. Kuno, P.V. Kamat, Shift happens. How halide ion defects influence photoinduced segregation in mixed halide perovskites, ACS Energy Lett. 2 (7) (2017) 1507–1514.
[22] L.A. Muscarella, E.M. Hutter, F. Wittmann, Y.W. Woo, Y.-K. Jung, L. McGovern, J. Versluis, A. Walsh, H.J. Bakker, B. Ehrler, Lattice compression increases the activation barrier for phase segregation in mixed-halide perovskites, ACS Energy Lett. 5 (10) (2020) 3152–3158.
[23] D.T. Limmer, N.S. Ginsberg, Photoinduced phase separation in the lead halides is a polaronic effect, J. Chem. Phys. 152 (23) (2020) 230901.
[24] J.T. DuBose, P.S. Mathew, J. Cho, M. Kuno, P.V. Kamat, Modulation of photo-induced iodine expulsion in mixed halide perovskites with electrochemical bias, J. Phys. Chem. Lett. 12 (2021) 2615–2621.
[25] J. Cho, P.V. Kamat, How chloride suppresses photoinduced phase segregation in mixed halide perovskites, Chem. Mater. 32 (14) (2020) 6206–6212.
[26] M.C. Brennan, A. Ruth, P.V. Kamat, M. Kuno, Photoinduced anion segregation in mixed halide perovskites, Trends Chem. 2 (4) (2020) 282–301.

[27] T. Elmelund, B. Seger, M. Kuno, P.V. Kamat, How interplay between photo and thermal activation dictates halide ion segregation in mixed halide perovskites, ACS Energy Lett. 5 (1) (2019) 56−63.
[28] T. Sheikh, A. Nag, Mn doping in centimeter-sized layered 2D Butylammonium lead bromide (BA2PbBr4) single crystals and their optical properties, J. Phys. Chem. C 123 (14) (2019) 9420−9427.
[29] P.S. Mathew, J.T. DuBose, J. Cho, P.V. Kamat, Spacer cations dictate photoinduced phase segregation in 2D mixed halide perovskites, ACS Energy Lett. 6 (2021) 2499−2501.
[30] W. Fan, Y. Shi, T. Shi, S. Chu, W. Chen, K.O. Ighodalo, J. Zhao, X. Li, Z. Xiao, Suppression and reversion of light-induced phase separation in mixed-halide perovskites by oxygen passivation, ACS Energy Lett. 4 (9) (2019) 2052−2058.
[31] F. Ruf, P. Rietz, M.F. Aygüler, I. Kelz, P. Docampo, H. Kalt, M. Hetterich, The bandgap as a moving target: reversible bandgap instabilities in multiple-cation mixed-halide perovskite solar cells, ACS Energy Lett. 3 (12) (2018) 2995−3001.
[32] G.F. Samu, Á. Balog, F. De Angelis, D. Meggiolaro, P.V. Kamat, C. Janáky, Electrochemical hole injection selectively expels iodide from mixed halide perovskite films, J. Am. Chem. Soc. 141 (27) (2019) 10812−10820.
[33] J. Yang, Z. Yuan, X. Liu, S. Braun, Y. Li, J. Tang, F. Gao, C. Duan, M. Fahlman, Q. Bao, Oxygen-and water-induced energetics degradation in organometal halide perovskites, ACS Appl. Mater. Interfaces 10 (18) (2018) 16225−16230.
[34] P.S. Mathew, G.F. Samu, C. Janáky, P.V. Kamat, Iodine (I) expulsion at photo-irradiated mixed halide perovskite interface. Should I stay or should I go? ACS Energy Lett. 5 (6) (2020) 1872−1880.
[35] J. Cho, P.S. Mathew, J.T. DuBose, P.V. Kamat, Photoinduced halide segregation in ruddlesden−popper 2D mixed halide perovskite films, Adv. Mater. 33 (48) (2021) 2105585.
[36] J.T. DuBose, P.V. Kamat, TiO2-assisted halide ion segregation in mixed halide perovskite films, J. Am. Chem. Soc. 142 (11) (2020) 5362−5370.
[37] S.K. Gautam, M. Kim, D.R. Miquita, J.E. Bourée, B. Geffroy, O. Plantevin, Reversible Photoinduced Phase Segregation and Origin of Long Carrier Lifetime in Mixed-Halide Perovskite Films, Adv. Functional Mater. (2020) 2002622.
[38] F. Peña-Camargo, P. Caprioglio, F. Zu, E. Gutierrez-Partida, C.M. Wolff, K. Brinkmann, S. Albrecht, T. Riedl, N. Koch, D. Neher, Halide segregation versus interfacial recombination in bromide-rich wide-gap perovskite solar cells, ACS Energy Lett. 5 (8) (2020) 2728−2736.